Efficient Method for Twist-Averaged Coupled Cluster Calculation of Gap Energy: Bulk Study of Stannic Oxide

Maliheh Shaban Tameh,

Wayne L. Gladfelter, Jason Goodpaster,*

Department of Chemistry

University of Minnesota

Minneapolis, Minnesota 55455

* Emails: jason@jdgoodpaster.com;jgoodpas@umn.edu;wlg@umn.edu

Abstract

We study gap energy of the semiconducting oxide SnO_2 through ab-initio calculations. DFT and coupled cluster calculations are presented and discussed. In this work, we emphasize that GGA+U does not improve the physics of the semicore *d* electrons in SnO_2. We report an overestimation in the gap energy by finite-size scaling at the thermodynamic limit through equation-of-motion (EOM) CCSD calculations. To address one-body and many-body errors, we report a combination of the Kwee-Zhang-Krakauer[1] (KZK) approach with twist averaging to explain twist averaged EOM-CCSD gap energy. In this approach, the correction to the gap energy originates from the difference between mean-field and many-body approximations and at the end the difference is added to the mean-filed gap of an infinite system to estimate the many-body gap in the thermodynamic limit. The efficiency of the twist averaging in reducing the finite-size errors is tested through different functionals.

I. Introduction

SnO_2 in the category of post-transition-metal oxides is used as transparent conducting oxides (TCOs) that are materials with specific features of high electrical conductivity and optical transparency in the visible range. These unique properties make SnO_2[2] a material with a variety of applications including optoelectronic devices,[3] transparent transistors[4-6] and solid state gas sensors.[7, 8] Due to such aspects, the electrical and optical properties of SnO_2 have been subjects of many experimental and theoretical studies. Accordingly, owing to a correlation between transparency and band gap of SnO_2, a detailed understanding of its electronic structure is essential.

Band gap energy of SnO_2 has been widely studied experimentally and theoretically. However, the results are contradictory and inconclusive. In Table I, we summarize reported theoretical and experimental band gap energies through different approaches.

In interpretation of adsorption measurements in SnO_2, there have been controversies regarding the symmetry of top valence band and values of transitions from the valence band to the conduction band. To clear up the argument, Nagasawa et al,[9] Agekyan,[10] and Fröhlich et al.[11] established a direct–forbidden minimum gap of 3.6 eV at Γ, where the highest valence band had Γ_3^+ symmetry. From the theoretical point of view, there have been intensive attempts to study the electronic structure of SnO_2, where most of them indicate that a direct gap takes place at Γ but the two lowest energy direct transitions are dipole–forbidden. Although dipole transitions are symmetry forbidden in single photon optical absorption, there are dipole-allowed transitions in two-photon absorption, where the measured value of ~3.6 eV has been reported.

In SnO_2, local density approximation (LDA), generalized gradient approximation (GGA), meta–GGAs, or van der Waals corrected functionals are known to underestimate the binding energy of the Sn d states. Hence, the calculated gaps based on the LDA[12-19] and the GGA[20-22] are assumed to suffer from theoretical deficiencies. Recently, the many–body perturbation theory calculations of the quasiparticle band structure within GW approximation have attracted attentions to address the band gap of SnO_2.[17, 23-26] Even though, an overestimation in band gap measurement has been pointed out,[26, 27] the calculations based on HSE03+G_0W_0 method show a fundamental gap close to the experimentally approved optical gap. A behavior that is assigned to the dipole–allowed direct transitions in the vicinity of the VBM at Γ. Besides, Sabino et al.[25] demonstrated that optical light intensity significantly influences the optical gap. Intense illumination is correlated with weak transition which is identified as the fundamental gap theoretically and agrees with experimental

optical gap measurements. Low illumination shows high-amplitude transitions at the Γ point, yielding an optical gap wider than the fundamental gap (4.34 eV instead of 3.60 eV). Based on their study, the very weak absorption in the vicinity of the Γ point at the band edges is originated from strong illumination that subsequently leads to the coincidence between the fundamental and optical gaps. However, the difference between fundamental and optical gaps under low illumination conditions is an open question. In this work, we intend to provide a better description of the gap energy of SnO_2 using coupled cluster calculations.

High level theories, e.g., hybrid functionals or GGA+U are known[28, 29] to correct the position of the d states. Nonetheless, many factors such as the amount of exact exchange in hybrid functionals and the underlying GGA along with the value of *U* parameter in GGA+U might affect the electronic structure properties. Therefore, it is assumed that there is a large uncertainty in the position of the defect level. Due to the full *d* states in SnO_2, GGA+U[30] does not provide correct description of the band gap and electronic properties of different species, a subject that was ignored in previous studies[17, 19, 30-33] and we address in our work. In contrast to GGA+U, it has been shown that mixing an amount of Fock exchange with DFT exchange can improve the description of localized electron states.[28, 34-37] Forms of Heyd–Scuseria–Ernzerhof (HSE) short–range screened hybrid[38, 39] that incorporate a fraction of Hartree–Fock (HF) exchange are well–stablished and in wide–spread use. These functionals yield an agreement between accuracy and computational cost. Besides, full–range hybrids such as B3PW91 have shown adequate efficiency in band gap prediction of semiconductors.[40]

Here, we provide a comprehensive theoretical study of the band gap of SnO_2 through ab initio calculations. At DFT level, we benchmark B3LYP, HSE06, PBE0,[41] and B3PW91 to calculate the band gap of SnO_2, where the performance of short–range and full–range hybrids are evaluated. On

the other hand, we apply the lowest–order truncation in the coupled–cluster (CC) theory of the Green's function, namely, equation–of–motion CC theory with single and double excitations (EOM–CCSD) to estimate band gap energy of SnO_2. We confirm how sensitive the electronic structure can be relative to the applied theoretical method. Here, an emphasis is given to the different behavior of the XC functionals in the two distinct codes of Vienna Ab-initio Simulation Package (VASP)[42, 43] and Python-based simulations of chemistry framework (PySCF).[44]

The rest of the paper is organized as follows. A description of the methodology is given in Sec. II. In Sec III we present and analyze our CCSD calculations which focus on the gap energy of SnO_2. The reliability and validity of the applied methods are discussed in this section. The conclusion is given in Sec IV.

II. Computational details

Tetragonal rutile unit cell of SnO_2 includes six atoms and is represented by two lattice parameters a and c and the internal parameter of u.[45-49] Each tin atom is surrounded by a distorted octahedron of six oxygen atoms and each oxygen atom has three tins nearest neighbors at the corners of an almost equilateral triangle. To obtain bulk equilibrium structure, geometry is relaxed with respect to the lattice a and internal parameter u using Vienna Ab-initio Simulation Package (VASP)[43] with Perdew–Burke–Ernzerhof (PBE)[50] functional and kinetic energy cutoff of 400 eV and 16×16×16 Monkhorst–Pack[51] **k**–points mesh. Our relaxed lattice parameters of $a = b = 4.827$ and $c = 3.246$ $^{\circ}A$, agree with the experimentally[48, 49] measured values of 4.737 and 3.186 $^{\circ}A$, respectively and generates experimental c/a ratio of 0.673.

We use DZVP and SBKJC–VDZ basis for tin and oxygen atoms to obtain basis set convergence. For the former basis, the calculations are equipped with Goedecker–Teter–Hutter (GTH) type

pseudopotentials constructed with the Perdew-Burke-Ernzerhof (PBE)[41] XC functional for all atoms. For the latter basis, core electrons of tin atoms are treated using the SBKJC ECP. CC calculations are performed based on the restricted HF orbitals. In all calculations, the Brillouin zone is sampled with a uniform Monkhorst–Pack mesh of N_k **k**–points. For twist averaging boundary condition calculations, we select 5 × 5 × 5 Monkhorst–Pack grid offsetted from the Γ point, where the Baldereschi[52] point (1/4, 1/4, 1/4) in the reciprocal coordinate is used to offset the twist grid. Within the periodic CC theory, the band gap is given by the calculation of the ionization potential (IP-EOM-CCSD) and the electron affinity (EA-EOM-CCSD).

Table I. Prior reports on SnO_2 band gap calculated within DFT, MBPT (many-body perturbation theory), and experiments.

Method	References	Gap (eV)
PP within LDA	ELP. Y Blancá et al.[18]	1.08
ASW within LDA	K. C. Mishra et al.[53]	3.70
PP within LDA	Y. Mi et al.[12]	0.70
PP within LDA	M. A. Mäki-Jaskari et al.[13]	1.35
USP within LDA	M. A. Mäki-Jaskari et al.[13]	1.68
LCAO within PBE	R. A. Evarestov et al.[54]	0.70
LCAO within B3LYP	R. A. Evarestov et al.[54]	4.03
FP-LAPW within LDA	L. A. Errico[15]	1.70
PAW within GGA	A. K. Singh et al.[30]	0.95
PAW within GGA+U	A. K. Singh et al.[14, 30]	1.65
USP within LDA	Z. Q. Li et al.[14]	1.20
USP within PW91	Q. J. Liu et al.[21]	0.13
PAW within HSE	J. B. Varley et al.[55]	3.50

PP within LDA	R. Saniz et al.[16]	1.80
PP within GW	R. Saniz et al.[16]	3.85
COHSEX + G_0W_0	J. A. Berger et al.[56]	3.80
PAW within PBE	P. D. Borges et al.[17, 57]	0.65
PAW within LDA+U	A. Schleife et al.[17]	1.19
PAW within G_0W_0 @ HSE03	A. Schleife et al.[17]	3.65
USP within PBE	L. Peng.Fei et al.[22]	1.15
PAW within GGA+U	Y. Kang et al.[32]	1.30
PAW within G_0W_0	Y. Kang et al.[32]	3.10
PAW within GW_0	Y. Kang et al.[32]	3.43
PAW within $QPGW_0$	Y. Kang et al.[32]	3.78
PAW within G_0W_0 @ HSE06	Y. Kang et al.[32]	3.89
PP within PBE0	E. Ching-Prado et al.[58]	3.62
Two-photon spectroscopy	D. Fröhlich et al.[11]	3.56
Two-photon spectroscopy	K. Reimann et al.[59]	3.59
Two-photon spectroscopy	M. Nagasawa et al.[9]	3.59
Two-photon spectroscopy	C. Schweizer[60]	3.59
Experiment	E. E. Kohnke[61]	3.70
Experiment	C. Terrier et al.[62]	4. $\pm$ 0.2
Experiment	W. Spence[62]	4.3

PP indicates Pseudopotentials. USP is ultrasoft pseudopotentials. LCAO is a linear combination of atomic orbitals. ASW is Augmented-spherical-wave. COHSEX is a Coulomb-hole plus screened exchange.

A. finite size errors

Uncertainty that arises from finite-size (FS) errors is correlated with finite simulation cells in simulation of materials. These errors are defined as the difference between the thermodynamic limit (TDL) and the finite simulation cell results. To reach accurate and reliable outcomes in exploring electronic structure quantities, an appropriate treatment of the FS errors is important. In periodic systems, the accuracy of the ab initio calculations depends on the size of the primitive cell. FS errors due to finite simulation cells can be reduced by the Bloch theorem, where the Brillouin zone (BZ) of the reciprocal lattice is spanned by enough boundary conditions, or **k**-points to ensure the reliability of the probing quantities. Technically, many samplings can reduce the one-body (independent particle) FS errors (non-interacting kinetic, potential, Hartree energies, etc.) arising from incomplete **k**–points grid. Twist averaging is a well established method to reduce these errors and facilitates the extrapolation to the TDL. Integrating a periodic function over the BZ is performed at every **k**-point. In this method, the **k**–points grid being offset from the origin by $\mathbf{k}_s$ twist vectors, which is called twisted boundary conditions and then one takes average of the expectation values of observables over all offsets, i.e., over the Bloch vectors $\mathbf{k}_s$ in the first BZ of the simulation cell that is called twist averaging boundary condition (TABC).

Here, we apply twist averaged boundary conditions (TABC) to eliminate single-particle errors. The twists can be chosen from a uniform Monkhorst-Pack grid, Baldereschi points, and high symmetry points, where offsetting from Γ may make other choices. Indeed, an insightful choice of the twists can reduce the cost while preserving accuracy.[63] Baldereschi point which is a special point in the BZ provides an energy very close to the one obtained by averaging over $\mathbf{k}_s$ in the Brillouin zone.

Spurious Coulomb interaction between periodic images is another source of the FS errors, which is also known as many-body contribution. These errors are not eliminated by twist averaging. Although, employment of large supercells can address such errors, it is impractical due to the cost and slow convergence. The Kwee-Zhang-Krakauer[1] (KZK) approach is among the other techniques to reduce or cancel such FS errors; this method includes FS corrections in DFT calculations with *finite-size* functionals. We utilize this scheme to exploit corrections based on DFT calculations to mimic the EOM-CCSD many-body errors. Indeed, the correction to the gap energy originates from the difference between mean-field and many-body approximations. This difference is then applied to the mean-filed gap of an infinite system to estimate the many-body gap in the thermodynamic limit.[64]

To address one-body and many-body contributions, we consider a combination of the KZK method with twist averaging which first was introduced by S. Azadi.[65] Here, we explain the twist averaged EOM-CCSD band gap energy augmented with KZK technique of the infinite simulation cell within this framework as follows.

$$\mathrm{G}^{\mathrm{CCSD}}_{\mathrm{TABC-KZK}(\infty)} = \mathrm{G}^{\mathrm{CCSD}}_{\mathrm{twstavrg}}(\mathrm{L}) + \Delta\mathrm{G}^{\mathrm{FS}}_{\mathrm{twstavrg}}(\mathrm{L}), \quad (1)$$

where, the first term is the twist averaged CCSD energy for a simulation cell of size L and the second term is the FS correction based on DFT calculations. Hence, one has

$$\mathrm{G}^{\mathrm{CCSD}}_{\mathrm{TABC-KZK}(\infty)} = \frac{1}{\mathrm{N}}\sum_{\mathbf{k}_\mathrm{s}} \mathrm{G}^{\mathrm{CCSD}}(\mathrm{L}, \mathbf{k}_\mathrm{s}) - \frac{1}{\mathrm{N}}\sum_{\mathbf{k}_\mathrm{s}} \mathrm{G}^{\mathrm{DFT,FS}}(\mathrm{L}, \mathbf{k}_\mathrm{s}) + \mathrm{G}^{\mathrm{DFT}}(\infty), \quad (2)$$

in which, N is the twist number, $\mathrm{G}^{\mathrm{DFT}}(\infty)$ is the DFT gap computed using a fully converged $\mathbf{k}$–points. The FS DFT gap, $\mathrm{G}^{\mathrm{DFT,FS}}(\mathrm{L}, \mathbf{k}_\mathrm{s})$ indicates twist averaged DFT gap using the same simulation cell and twists as CCSD twist averaged calculations. Interestingly, FS correction addresses all FS errors.

III. Results and discussions

1. GGA+U

To describe the strong Coulomb interactions by the electrons in the d shell of the cation in SnO_2, the on–site Coulomb self–interaction potential is given by the GGA+*U* approach. In this theory, the electronic structure is divided into two subsystems of localized and delocalized states. The Coulomb *d–d* interactions between localized electrons of the same atomic center are treated via a Hartree–Fock–like approach and the interactions between delocalized *s* and *p* electrons are treated with GGA in the framework of DFT. Indeed, the majority of the intra–atomic self–interaction error is addressed by the HF theory that reduces the overestimation of the binding energy of the localized electrons in d shell and therefore, gives rise to a decrease in the *p–d* coupling. The performance of this method lies in the choice of parameter *U*, for which two methods have been assigned. In the first method, this parameter is referred to as a tuning parameter, for which the validity is tested versus known properties of the system of interest. Even though this approach generates reasonable results, it lacks a theoretical support that limits its applicability in systems without solid experimental data. The other case is known as the linear response approach introduced by Cococcioni and Gironcoli[96] that is based on DFT calculations, whereby a correction term is added to the energy. Hubbard correction based on the *U* is defined as $E_U[n^{i\sigma}] = \sum_{i\sigma} \frac{U^i}{2} Tr[n^{i\sigma}(1 - n^{i\sigma})]$, where E_U is the Hubbard correction and $n^{i\sigma}$ is the electron occupation at site *i* with spin σ. This term incorporates into the GGA portion. A value of *U* parameter corresponds to the second derivative $(\frac{\partial^2 E}{\partial n^2})$ of the ground state energy $(E(n))$ or the level change with respect to occupation, $\frac{\partial \epsilon}{\partial n}$. An effective Coulomb interaction parameter *U* is given by $U = \chi_0^{-1} - \chi^{-1}$, where $\chi_0 = \frac{\partial n}{\partial \alpha^{KS}}$ and $\chi = \frac{\partial n}{\partial \alpha}$ are the bare and interacting response coefficient obtained from the linear relationship

between orbital occupation and Lagrange multiplier (α). In fact, Lagrange multiplier (α) is the local perturbation potential that is applied to the localized states. Based on the linear character of this relationship, the perturbation of α in a narrow range would lead to a linear regression of orbital occupation (n) versus α. So, we can determine χ_0 and χ. This method addresses the self–interaction error (SIE) or delocalization error in the Hartree term. In the meanwhile, it has low computational cost. Our analysis shows that perturbation of O–*p* orbital has no influence on the Sn orbitals. Furthermore, Sn–*d* perturbation does not induce the oxygen and the Sn atoms therefore, no response is received. To summarize, the perturbation used to compute the *U* parameter has no effect on the tin's occupations and the oxygen. We attribute this behavior to the full Sn–*d* orbital that cannot be well described by the GGA+*U*. Although, the efficiency of this method has been proven on strongly correlated electron materials (SCEM) that contain many electrons in partially filled *d* or *f* shells, similar attempts have been made on wide–band gap semiconductors with filled bands of semicore states. Whereas GGA+*U* does not improve the physics of the semicore *d* electrons in these systems, a better correction is rendered to the cases with 3*d* states compared to those of 4*d* states that is attributed to a larger localization in these states.

2. Thermodynamic limit (TDL) and twist averaging boundary condition (TABC): EOM-CCSD and DFT calculations.

In Table II, we present the direct gap values at Γ within DFT and EOM–CCSD formalisms using PySCF package. For DFT calculations we use PBE0, the B3LYP, and the B3PW91 hybrid functionals. The band gap values are given with a n × n × n sampling of the Brillouin zone, where n varies from 1 to 5. Utmost DFT calculations use a 3 × 3 × 3 sampling with the DZVP basis set for all atoms and 5 × 5 × 5 sampling with the DZVP basis set for the O atoms and the SBKJC

basis set for the Sn atoms. The reason lies in the fact that the cost of CCSD calculations is very high, so we opt for SBKJC basis set for tin atoms to afford very demanding calculations. For the sake of comparison, we use the same basis set for DFT calculations as well. Therefore, there is a chance of testing the reliability of SBKJC over DZVP in our estimations.

We continue with this setting to obtain the EOM–CCSD gap. A comparison of DFT gap values given in Table II using $2 \times 2 \times 2$ and $3 \times 3 \times 3$ samplings with different basis sets of SBKJC and DZVP for Sn atoms, yields about 0.11 eV difference. Therefore, it is independent of the sampling of the Brillouin zone.

The extrapolation of the form of $N_k^{-1/3}$ is performed to reach the thermodynamic (or infinite-size) limit (TDL).[66] N_k is the number of the **k**-points in the mesh.

TABLE II. Band gap (eV) of SnO_2 using various settings of functional, code, basis set, and **k**–points.

Functional	Code	Basis set		**k**-points	Gap
		Sn	O		
EOM-CCSD	PySCF	SBKJC	Dzvp	$1 \times 1 \times 1$	1.03
		SBKJC	Dzvp	$2 \times 2 \times 2$	2.80
		SBKJC	Dzvp	$3 \times 3 \times 3$	3.32
		SBKJC	dzvp	Extrap,$N_k^{-1/3}$	4.36
PBE0	PySCF	dzvp	Dzvp	$1 \times 1 \times 1$	0.85
		dzvp	Dzvp	$2 \times 2 \times 2$	2.00
		dzvp	Dzvp	$3 \times 3 \times 3$	2.32
		dzvp	dzvp	Extrap,$N_k^{-1/3}$	3.15

		SBKJC	dzvp	$1 \times 1 \times 1$	1.02
		SBKJC	dzvp	$2 \times 2 \times 2$	2.12
		SBKJC	dzvp	$3 \times 3 \times 3$	2.43
		SBKJC	dzvp	$4 \times 4 \times 4$	2.60
		SBKJC	dzvp	$5 \times 5 \times 5$	2.69
		SBKJC	dzvp	Extrap,$N_k^{-1/3}$	3.07
		SBKJC	dzvp	TABC	3.02
B3LYP	PySCF	dzvp	dzvp	$1 \times 1 \times 1$	0.90
		dzvp	dzvp	$2 \times 2 \times 2$	1.97
		dzvp	dzvp	$3 \times 3 \times 3$	2.24
		dzvp	dzvp	Extrap,$N_k^{-1/3}$	3.04
		SBKJC	dzvp	$1 \times 1 \times 1$	1.05
		SBKJC	dzvp	$2 \times 2 \times 2$	2.08
		SBKJC	dzvp	$3 \times 3 \times 3$	2.34
		SBKJC	dzvp	$4 \times 4 \times 4$	2.47
		SBKJC	dzvp	$5 \times 5 \times 5$	2.55
		SBKJC	dzvp	Extrap,$N_k^{-1/3}$	2.86
		SBKJC	dzvp	TABC	2.86
B3PW91	PySCF	dzvp	dzvp	$1 \times 1 \times 1$	0.79
		dzvp	dzvp	$2 \times 2 \times 2$	1.80
		dzvp	dzvp	$3 \times 3 \times 3$	2.06

		dzvp	dzvp	Extrap,$N_k^{-1/3}$	2.81
		SBKJC	dzvp	$1 \times 1 \times 1$	0.97
		SBKJC	dzvp	$2 \times 2 \times 2$	1.91
		SBKJC	dzvp	$3 \times 3 \times 3$	2.17
		SBKJC	dzvp	$4 \times 4 \times 4$	2.30
		SBKJC	dzvp	$5 \times 5 \times 5$	2.38
		SBKJC	dzvp	Extrap,$N_k^{-1/3}$	2.69
		SBKJC	dzvp	TABC	2.69
PBE0	VASP			$2 \times 2 \times 2$	3.06
				$4 \times 4 \times 4$	2.97
				$6 \times 6 \times 6$	2.94
B3LYP	VASP			$2 \times 2 \times 2$	2.62
				$4 \times 4 \times 4$	2.55
				$6 \times 6 \times 6$	2.53
HSE06	VASP			$2 \times 2 \times 2$	2.29
				$4 \times 4 \times 4$	2.26
				$6 \times 6 \times 6$	2.26

To do the extrapolation we exclude the $1 \times 1 \times 1$ values. As is seen in Table II, the TDL introduces interesting consequence that we will focus on here. For the PBE0, B3LYP, and B3PW91 the TDL gap using DZVP basis set for Sn atom yields about 0.8 eV higher gap energy compared to the corresponding values from $3 \times 3 \times 3$ **k**-points calculations. A switch to SBKJ for Sn atom allows

us to increase the mesh to $5 \times 5 \times 5$, so the interpolations (TDL) yield lower average difference of 0.31 eV compared to the latest calculations with $5 \times 5 \times 5$ **k**-points. However, comparing the TDL values (Extrap,$N_k^{-1/3}$) for each functional of PBE0, B3LYP, and B3PW91 yields ~0.13 eV difference indicating that the TDL suggests reliable gap energies (at least in our case of study) considering the governing self-interaction error, the system size, and the quantum chemical method.

In Table II, the TABC values are based on the $5 \times 5 \times 5$ Monkhorst–Pack mesh and the Baldereschi point. It is seen that TABC estimations are in very close agreement with TDL gap values. Therefore, our estimations indicate that TABC with higher sampling is compatible with TDL. For instance, TABC calculations using 4×4×4 sampling and the Baldereschi point yields the same gap values of $4 \times 4 \times 4$ **k**–points, without employing any twist, that implies a deliberate sampling is needed to provide a correct description the gap values. Therefore, as the number of twists increase to infinity, the accuracy of the result is increased. Our results confirm that addressing finite-size errors in mean-field approaches (as DFT) can be easily achieved through twist averaging as the number of twists tends to infinity.

The performance of the extrapolation to reach TDL is shown in Figure 1. The solid and dashed lines (red, green, and purple) correspond to gap energies within DFT using DZVP and SBKJC for Sn atoms, respectively, in PySCF.

From the figure it is seen that irrespective of the type of applied basis set, all the estimations lie in the same range, evidence that we discussed it at above. Thus, a higher-level method that is not suffering from self-interaction errors is needed to give a correct description of the gap energies.

Blue dashed line in the Figure 1 denotes least-squares extrapolation with the form $N_k^{-1/3}$ using $2 \times 2 \times 2$ and $3 \times 3 \times 3$ values through CC method in order to obtain the gap energy.

Ab initio EOM-CCSD calculations in periodic systems is very computationally expensive. Indeed, it is not practical to go beyond $3 \times 3 \times 3$ **k**-points in our system. Using $3 \times 3 \times 3$ **k**-points, our estimated EOM-CCSD gap is 3.32 eV and the corresponding TDL EOM-CCSD is 4.36 eV. The EOM-CCSD's gap energy agrees with the corresponding gap of 3.6 eV from two photon absorption experiments and the TDL EOM-CCSD gap energy is overestimated about 0.8 eV. The large TDL indicates that the estimated finite-size effect is quite large.

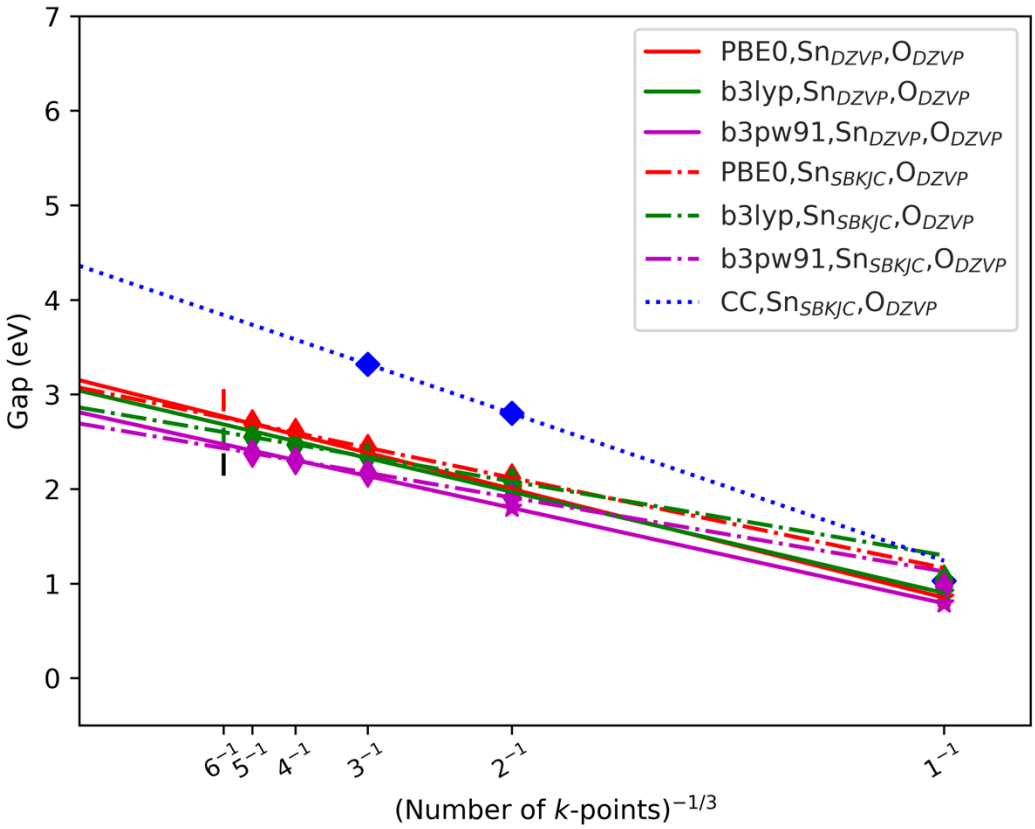

Figure 1. Band gap extrapolation for SnO_2. The dashed lines and solid lines represent least-squares extrapolation to the thermodynamic limit for each functional. The blue diamond show the CC gap values and the blue dashed line denotes least-squares extrapolation with the form $N_k^{-1/3}$. Red, green, and black vertical lines display values obtained by PBE0, B3LYP, and HSE06 functionals, respectively, within VASP code.

Within DFT, different hybrid functionals of PBE0, B3LYP, and HSE06, which differ by the portions of Hartree–Fock exchange, are used to calculate the gap and merit of them is evaluated. Results are presented in Table II. We compare the gap energies using both four and fourteen valence electrons, where in the later semicore Sn *d* states can be treated as valence states through the projector augmented wave (PAW) method. As including *d* states changes the gap by 0.08 eV using PBE0, we consider fourteen valence electrons for Sn atoms in our estimations. $6 \times 6 \times 6$ **k**–mesh is selected by convergence test. In Figure 1, red, green, and black vertical lines show gap for the corresponding PBE0, B3LYP, and HSE0 functionals. It is worthy to note that the converged values do not reflect TDL.

3. Twist averaged EOM-CCSD band gap energy augmented with KZK technique ($\mathbf{G}^{\mathbf{CCSD}}_{\mathbf{TABC-KZK}}(\infty)$)

As discussed in Sec. IIIA, to reduce or eliminate the FS errors, it is important to perform the calculations using a supercell and a dense mesh. However, these solutions may not be achievable and generalized. In EOM-CCSD, one should notice that an increase in the **k**–points sampling results in a slower convergence and the cost exceeds the computational resources. For the same reason, it is not always practical to utilize the supercell for EOM-CCSD calculations to increase the accuracy and reliability in probing electronic structure properties. Employment of supercell versus primitive cell to calculate the gap values of MnO and NiO within EOM-CCSD has been examined.[66]

In Table IV, we report twist averaged EOM-CCSD band gap energy augmented with KZK technique in equation 2, $G^{CCSD}_{TABC-KZK}(\infty)$, using different **k**–points sampling in $1 \times 1 \times 1$ cell. For Monkhorst$^{2\times2\times2}$ and Monkhorst$^{3\times3\times3}$ we use 8 and 27 points, respectively.

For Chadi & Cohen, four points of (1/8,1/8,1/8), (3/8,1/8,1/8), (3/8,3/8,1/8), (3/8,3/8,3/8) in addition to the Baldereschi point of (1/4,1/4,1/4) are used. High symmetry represents (1/2,1/2,1/2), (1/2,1/2,0), (0,1/2,1/2), (0,1/2,0), and (0,0,1/2) points which are **Γ**, **A**, **M**, **R**, **X**, **Z**, respectively, indicating symmetry **k**–points of tetragonal lattice. The PBE0, the B3LYP, and the B3PW91 hybrid functionals are used for the calculations in the second and the third terms in the equation 2. In G_{∞}^{DFT}, for the fully converged **k**–points mesh we use extrapolated gaps of 3.07, 2.86, and 2.69 eV for the PBE0, the B3LYP, and the B3PW91 functionals represented in Table II. Figure 2 represents EOM-CCSD gap energies augmented with KZK technique, $G_{TABC-KZK}^{CCSD}(\infty)$.

As is seen in Table IV, $G_{TABC-KZK}^{CCSD}(\infty)$ estimations are comparable using Monkhorst^{4x4x4} and Baldereschi point by all functionals. Our results indicate that to have a balance between the computational cost and accuracy the Baldereschi point, Chadi & Cohen are reliable choices.

For comparison purpose we consider 3.46, 3.24, and 3.20 eV using Monkhorst^{4x4x4} PBE0, the B3LYP, and the B3PW91 functionals. $G_{TABC-KZK}^{CCSD}(\infty)$ improves the extrapolated gaps in Table II by 0.31, 0.2, 0.39 (eV) using DZVP basis set for all atoms and PBE0, B3LYP, and B3PW91, respectively. Using SBKJ basis set for Sn and DZVP for O in the extrapolated gaps (Table II.), $G_{TABC-KZK}^{CCSD}(\infty)$ improves gaps by 0.39, 0.38, 0.51eV, for PBE0, B3LYP, and B3PW91, respectively. Therefore, even though $G_{TABC-KZK}^{CCSD}(\infty)$ suggest very reliable gap energies but still the effect of the applied DFT functional in the $G^{DFT}(\infty)$ term in equation 2 is observable. This can be easily explained as the DFT intrinsically error of G_{∞}^{DFT} in $G_{TABC-KZK}^{CCSD}(\infty)$ formulation, where the underestimation is much observable using G_{∞}^{PBE} in Table IV.

On the other hand, since to compute the gap energies using a fully converged **k**–points (selected from Table II) in $G^{DFT}(\infty)$ a 1 × 1 × 1 cell was used, we expect to suffer from an indirect influence in our estimations through $G_{TABC-KZK}^{CCSD}(\infty)$. However, our results indicate that twist averaged

EOM-CCSD band gap energy augmented with KZK technique based on PBE0 is in close agreement with the gap energy based on two photon spectroscopies shown in Table I.

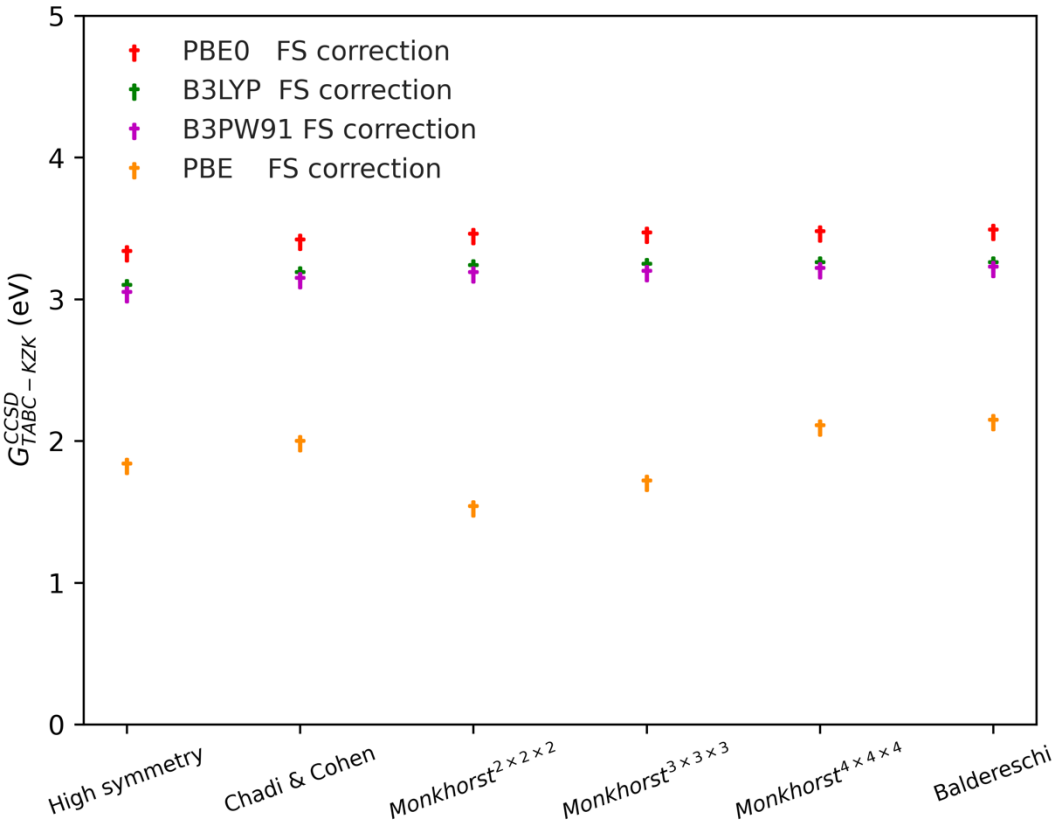

Figure 2. Twist averaged EOM-CCSD band gap energy augmented with KZK technique, $G^{CCSD}_{TABC-KZK}(\infty)$, using different **k**–points sampling and 1 × 1 × 1 cell. PBE0, B3LYP, and B3PW91 functionals are employed for FS DFT corrections in equation 2.

TABLE IV. Twist averaged EOM-CCSD band gap energy augmented with KZK technique, $G^{CCSD}_{TABC-KZK}(\infty)$, using different **k**–points sampling and 1 × 1 × 1 cell.

FS DFT method	k-points	$G^{CCSD}_{TABC-KZK}(\infty)$
PBE0	$Monkhorst^{2x2x2}$	3.44
	$Monkhorst^{3x3x3}$	3.45
	$Monkhorst^{4x4x4}$	3.46
	Chadi & Cohen	3.40
	High symmetry	3.32
	Baldereschi	3.47
B3LYP	$Monkhorst^{2x2x2}$	3.22
	$Monkhorst^{3x3x3}$	3.23
	$Monkhorst^{4x4x4}$	3.24
	Chadi & Cohen	3.17
	High symmetry	3.08
	Baldereschi	3.24
B3PW91	$Monkhorst^{2x2x2}$	3.17
	$Monkhorst^{3x3x3}$	3.18
	$Monkhorst^{4x4x4}$	3.20
	Chadi & Cohen	3.13
	High symmetry	3.03
	Baldereschi	3.21

IV. **Conclusion**

We presented ab initio study of the gap energy of SnO_2. Our work provided various ways to apply periodic coupled cluster methods. We reported twist averaged EOM-CCSD band gap energy augmented with KZK technique, $G^{CCSD}_{TABC-KZK}(\infty)$, using various sampling in the Brillouin zone. The optimal sampling points are introduced to reduce the cost of the twist averaging. The value of twist averaging in reducing the finite-size errors is addressed by using different functionals. Our results illustrate that we effectively addressed one-body and many-body errors in the gap energy estimation using $G^{CCSD}_{TABC-KZK}(\infty)$ approach. We find a fundamental gap of 3.46 eV for SnO_2 that is

in close agreement with two photon spectroscopy experiments. The gap obtained by EOM-CCSD is overestimated in the thermodynamic limit, indicating that the estimated finite-size effect is large.

Acknowledgment

This work is funded by a grant from the National Science Foundation (DMR 1607318). The authors acknowledge the Minnesota Supercomputing Institute (MSI) at the University of Minnesota for providing resources that contributed to research results reported within this paper.

Reference:

1. Kwee, H.; Zhang, S.; Krakauer, H., Finite-size correction in many-body electronic structure calculations. *Physical review letters* **2008,** *100* (12), 126404.
2. Wang, T.; Prakash, A.; Warner, E.; Gladfelter, W. L.; Jalan, B., Molecular beam epitaxy growth of SnO2 using a tin chemical precursor. *Journal of Vacuum Science & Technology A* **2015,** *33* (2).
3. Pan, S.; Ye, C.; Teng, X.; Fan, H.; Li, G., Preparation and characterization of nitrogen-incorporated SnO 2 films. *Applied Physics A* **2006,** *85*, 21-24.
4. Minami, T., Transparent conducting oxide semiconductors for transparent electrodes. *Semiconductor science and technology* **2005,** *20* (4), S35.
5. Granqvist, C. G., Transparent conductors as solar energy materials: A panoramic review. *Solar energy materials and solar cells* **2007,** *91* (17), 1529-1598.
6. Zhang, K. H.; Xi, K.; Blamire, M. G.; Egdell, R. G., P-type transparent conducting oxides. *Journal of Physics: Condensed Matter* **2016,** *28* (38), 383002.
7. Kohl, D., Surface processes in the detection of reducing gases with SnO2-based devices. *Sensors and actuators* **1989,** *18* (1), 71-113.
8. Gurlo, A., Interplay between O2 and SnO2: oxygen ionosorption and spectroscopic evidence for adsorbed oxygen. *ChemPhysChem* **2006,** *7* (10), 2041-2052.
9. Nagasawa, M.; Shionoya, S., Urbach's rule exhibited in SnO2. *Solid State Communications* **1969,** *7* (23), 1731-1733.
10. Agekyan, V., Spectroscopic properties of semiconductor crystals with direct forbidden energy gap. *physica status solidi (a)* **1977,** *43* (1), 11-42.
11. Fröhlich, D.; Kenklies, R.; Helbig, R., Band-Gap Assignment in Sn O 2 by Two-Photon Spectroscopy. *Physical Review Letters* **1978,** *41* (25), 1750.
12. Mi, Y. M. Y.; Odaka, H. O. H.; Iwata, S. I. S., Electronic structures and optical properties of ZnO, SnO2 and In2O3. *Japanese journal of applied physics* **1999,** *38* (6R), 3453.
13. Mäki-Jaskari, M. A.; Rantala, T. T., Band structure and optical parameters of the SnO 2 (110) surface. *Physical Review B* **2001,** *64* (7), 075407.

14. Li, Z.; Yin, Y.; Liu, X.; Li, L.; Liu, H.; Song, Q., Electronic structure and optical properties of Sb-doped SnO2. *Journal of Applied Physics* **2009,** *106* (8).
15. Errico, L. A., Ab initio FP-LAPW study of the semiconductors SnO and SnO2. *Physica B: Condensed Matter* **2007,** *389* (1), 140-144.
16. Saniz, R.; Dixit, H.; Lamoen, D.; Partoens, B., Quasiparticle energies and uniaxial pressure effects on the properties of SnO2. *Applied Physics Letters* **2010,** *97* (26).
17. Schleife, A.; Varley, J.; Fuchs, F.; Rödl, C.; Bechstedt, F.; Rinke, P.; Janotti, A.; Van de Walle, C., Tin dioxide from first principles: Quasiparticle electronic states and optical properties. *Physical Review B* **2011,** *83* (3), 035116.
18. y Blancá, E. P.; Svane, A.; Christensen, N.; Rodriguez, C.; Cappannini, O.; Moreno, M., Calculated static and dynamic properties of β-Sn and Sn-O compounds. *Physical Review B* **1993,** *48* (21), 15712.
19. Shi, L.-B.; Dong, H.-K.; Qi, G.-Q., Density functional theory description of origin of ferromagnetism in Cu doped SnO2. *Journal of magnetism and magnetic materials* **2013,** *345*, 215-221.
20. Yamaguchi, Y.; Tabata, K.; Yashima, T., First-principles calculations on the surface electronic and reactive properties of M/SnO2 (M= Ge, Mn)(110). *Journal of Molecular Structure: Theochem* **2005,** *714* (2-3), 221-233.
21. Liu, Q.-J.; Liu, Z.-T.; Feng, L.-P., First-principles calculations of structural, electronic and optical properties of tetragonal SnO2 and SnO. *Computational materials science* **2010,** *47* (4), 1016-1022.
22. Lu, P.-F.; Shen, Y.; Yu, Z.-Y.; Zhao, L.; Li, Q.-Y.; Ma, S.-J.; Han, L.-H.; Liu, Y.-M., Electronic structure and optical properties of antimony-doped SnO2 from first-principle study. *Communications in Theoretical Physics* **2012,** *57* (1), 145.
23. Shishkin, M.; Marsman, M.; Kresse, G., Accurate quasiparticle spectra from self-consistent GW calculations with vertex corrections. *Physical review letters* **2007,** *99* (24), 246403.
24. Berger, J.; Reining, L.; Sottile, F., Efficient G W calculations for SnO 2, ZnO, and rubrene: The effective-energy technique. *Physical Review B* **2012,** *85* (8), 085126.
25. Sabino, F. P.; Oliveira, L. N.; Wei, S.-H.; Da Silva, J. L., Optical and fundamental band gaps disparity in transparent conducting oxides: New findings for the and systems. *Journal of Physics: Condensed Matter* **2017,** *29* (8), 085501.
26. Cai, X.; Zhang, P.; Wei, S.-H., Revisit of the band gaps of rutile SnO2 and TiO2: A first-principles study. *Journal of Semiconductors* **2019,** *40* (9), 092101.
27. Chen, W.; Pasquarello, A., Band-edge positions in G W: Effects of starting point and self-consistency. *Physical Review B* **2014,** *90* (16), 165133.
28. Janotti, A.; Van de Walle, C. G., LDA+ U and hybrid functional calculations for defects in ZnO, SnO2, and TiO2. *physica status solidi (b)* **2011,** *248* (4), 799-804.
29. Scanlon, D. O.; Dunnill, C. W.; Buckeridge, J.; Shevlin, S. A.; Logsdail, A. J.; Woodley, S. M.; Catlow, C. R. A.; Powell, M. J.; Palgrave, R. G.; Parkin, I. P., Band alignment of rutile and anatase TiO2. *Nature materials* **2013,** *12* (9), 798-801.
30. Singh, A. K.; Janotti, A.; Scheffler, M.; Van de Walle, C. G., Sources of electrical conductivity in SnO 2. *Physical review letters* **2008,** *101* (5), 055502.
31. Canestraro, C. D.; Roman, L. S.; Persson, C., Polarization dependence of the optical response in SnO2 and the effects from heavily F doping. *Thin Solid Films* **2009,** *517* (23), 6301-6304.

32. Kang, Y.; Kang, G.; Nahm, H.-H.; Cho, S.-H.; Park, Y. S.; Han, S., G W calculations on post-transition-metal oxides. *Physical Review B* **2014,** *89* (16), 165130.
33. Ding, S.-S.; Huang, W.-Q.; Yang, Y.-C.; Zhou, B.-X.; Hu, W.-Y.; Long, M.-Q.; Peng, P.; Huang, G.-F., Dual role of monolayer MoS2 in enhanced photocatalytic performance of hybrid MoS2/SnO2 nanocomposite. *Journal of Applied Physics* **2016,** *119* (20).
34. Yamaguchi, Y.; Nagasawa, Y.; Murakami, A.; Tabata, K., Stability of oxygen anions and hydrogen abstraction from methane on reduced SnO2 (110) surface. *International journal of quantum chemistry* **1998,** *69* (5), 669-678.
35. Di Valentin, C.; Pacchioni, G.; Selloni, A., Electronic structure of defect states in hydroxylated and reduced rutile TiO 2 (110) surfaces. *Physical review letters* **2006,** *97* (16), 166803.
36. Janotti, A.; Varley, J.; Rinke, P.; Umezawa, N.; Kresse, G.; Van de Walle, C., Hybrid functional studies of the oxygen vacancy in TiO 2. *Physical Review B* **2010,** *81* (8), 085212.
37. Lee, H.-Y.; Clark, S. J.; Robertson, J., Calculation of point defects in rutile TiO 2 by the screened-exchange hybrid functional. *Physical Review B* **2012,** *86* (7), 075209.
38. Heyd, J.; Scuseria, G. E.; Ernzerhof, M., Hybrid functionals based on a screened Coulomb potential. *The Journal of chemical physics* **2003,** *118* (18), 8207-8215.
39. Paier, J.; Marsman, M.; Hummer, K.; Kresse, G.; Gerber, I. C.; Ángyán, J. G., Screened hybrid density functionals applied to solids. *The Journal of chemical physics* **2006,** *124* (15).
40. Garza, A. J.; Scuseria, G. E., Predicting band gaps with hybrid density functionals. *The journal of physical chemistry letters* **2016,** *7* (20), 4165-4170.
41. Perdew, J. P.; Ernzerhof, M.; Burke, K., Rationale for mixing exact exchange with density functional approximations. *The Journal of chemical physics* **1996,** *105* (22), 9982-9985.
42. Kresse, G.; Hafner, J., Ab initio molecular dynamics for liquid metals. *Physical review B* **1993,** *47* (1), 558.
43. Hafner, J., Ab-initio simulations of materials using VASP: Density-functional theory and beyond. *Journal of computational chemistry* **2008,** *29* (13), 2044-2078.
44. Sun, Q.; Berkelbach, T. C.; Blunt, N. S.; Booth, G. H.; Guo, S.; Li, Z.; Liu, J.; McClain, J. D.; Sayfutyarova, E. R.; Sharma, S., PySCF: the Python-based simulations of chemistry framework. *Wiley Interdisciplinary Reviews: Computational Molecular Science* **2018,** *8* (1), e1340.
45. Oviedo, J.; Gillan, M., First-principles study of the interaction of oxygen with the SnO2 (1 1 0) surface. *Surface Science* **2001,** *490* (3), 221-236.
46. Sensato, F. R.; Custódio, R.; Calatayud, M.; Beltrán, A.; Andrés, J.; Sambrano, J. R.; Longo, E., Periodic study on the structural and electronic properties of bulk, oxidized and reduced SnO2 (1 1 0) surfaces and the interaction with O2. *Surface Science* **2002,** *511* (1-3), 408-420.
47. Rantala, T. T.; Rantala, T. S.; Lantto, V., Surface relaxation of the (110) face of rutile SnO2. *Surface Science* **1999,** *420* (1), 103-109.
48. Baur, W. H., Über die verfeinerung der kristallstrukturbestimmung einiger vertreter des rutiltyps: TiO2, SnO2, GeO2 und MgF2. *Acta Crystallographica* **1956,** *9* (6), 515-520.
49. Haines, J.; Léger, J., X-ray diffraction study of the phase transitions and structural evolution of tin dioxide at high pressure: ffRelationships between structure types and implications for other rutile-type dioxides. *Physical Review B* **1997,** *55* (17), 11144.
50. Perdew, J. P.; Burke, K.; Ernzerhof, M., Generalized gradient approximation made simple. *Physical review letters* **1996,** *77* (18), 3865.

51. Monkhorst, H. J.; Pack, J. D., Special points for Brillouin-zone integrations. *Physical review B* **1976,** *13* (12), 5188.
52. Baldereschi, A., Mean-value point in the Brillouin zone. *Physical Review B* **1973,** *7* (12), 5212.
53. Mishra, K.; Johnson, K.; Schmidt, P., Electronic structure of antimony-doped tin oxide. *Physical Review B* **1995,** *51* (20), 13972.
54. Evarestov, R.; Bandura, A.; Proskurov, E., Plain DFT and hybrid HF-DFT LCAO calculations of SnO2 (110) and (100) bare and hydroxylated surfaces. *physica status solidi (b)* **2006,** *243* (8), 1823-1834.
55. Varley, J.; Janotti, A.; Van de Walle, C., Group-V impurities in SnO 2 from first-principles calculations. *Physical Review B* **2010,** *81* (24), 245216.
56. Berger, J.; Reining, L.; Sottile, F., Ab initio calculations of electronic excitations: Collapsing spectral sums. *Physical Review B* **2010,** *82* (4), 041103.
57. Borges, P. D.; Scolfaro, L. M.; Leite Alves, H. W.; da Silva, E. F., DFT study of the electronic, vibrational, and optical properties of SnO 2. *Theoretical Chemistry Accounts* **2010,** *126*, 39-44.
58. Ching-Prado, E.; Samudio, C.; Santiago-Aviles, J.; Velumani, S., Electronic structure and optical properties of SnO 2: F from PBE0 hybrid functional calculations. *Journal of Materials Science: Materials in Electronics* **2018,** *29*, 15423-15435.
59. Reimann, K.; Steube, M., Experimental determination of the electronic band structure of SnO2. *Solid State Communications* **1998,** *105* (10), 649-652.
60. Schweitzer, C.; Reimann, K.; Steube, M., Two-photon spectroscopy of SnO2 under hydrostatic pressure. *Solid state communications* **1999,** *110* (12), 697-700.
61. Kohnke, E., Electrical and optical properties of natural stannic oxide crystals. *Journal of Physics and Chemistry of Solids* **1962,** *23* (11), 1557-1562.
62. Terrier, C.; Chatelon, J.; Roger, J., Electrical and optical properties of Sb: SnO2 thin films obtained by the sol-gel method. *Thin solid films* **1997,** *295* (1-2), 95-100.
63. Drummond, N.; Needs, R.; Sorouri, A.; Foulkes, W., Finite-size errors in continuum quantum Monte Carlo calculations. *Physical Review B* **2008,** *78* (12), 125106.
64. Azadi, S.; Drummond, N. D.; Foulkes, W. M. C., Nature of the metallization transition in solid hydrogen. *Physical Review B* **2017,** *95* (3), 035142.
65. Azadi, S.; Foulkes, W., Systematic study of finite-size effects in quantum Monte Carlo calculations of real metallic systems. *The Journal of chemical physics* **2015,** *143* (10).
66. Gao, Y.; Sun, Q.; Jason, M. Y.; Motta, M.; McClain, J.; White, A. F.; Minnich, A. J.; Chan, G. K.-L., Electronic structure of bulk manganese oxide and nickel oxide from coupled cluster theory. *Physical Review B* **2020,** *101* (16), 165138.